Remote Sensing of Environment 114 (2010) 1053–1068

Contents lists available at ScienceDirect

Remote Sensing of Environment

journal homepage: www.elsevier.com/locate/rse

Quantification of live aboveground forest biomass dynamics with Landsat time-series and field inventory data: A comparison of empirical modeling approaches

Scott L. Powell [a,*], Warren B. Cohen [b], Sean P. Healey [c], Robert E. Kennedy [d], Gretchen G. Moisen [c], Kenneth B. Pierce [e], Janet L. Ohmann [b]

[a] Department of Land Resources and Environmental Sciences, Montana State University, P.O. Box 173120, Bozeman, MT 59717, United States
[b] U.S.D.A. Forest Service, Pacific Northwest Research Station, 3200 SW Jefferson Way, Corvallis, OR 97731, United States
[c] U.S.D.A. Forest Service, Rocky Mountain Research Station, 507 25th St., Ogden, UT 84401, United States
[d] Department of Forest Science, Oregon State University, 321 Richardson Hall, Corvallis, OR 97731, United States
[e] Washington Department of Fish and Wildlife, 600 Capitol Way North, Olympia, WA 98501, United States

ARTICLE INFO

Article history:
Received 7 July 2009
Received in revised form 15 December 2009
Accepted 20 December 2009

Keywords:
Biomass
Landsat
FIA
Disturbance
Curve-fitting
Random forests

ABSTRACT

Spatially and temporally explicit knowledge of biomass dynamics at broad scales is critical to understanding how forest disturbance and regrowth processes influence carbon dynamics. We modeled live, aboveground tree biomass using Forest Inventory and Analysis (FIA) field data and applied the models to 20+ year time-series of Landsat satellite imagery to derive trajectories of aboveground forest biomass for study locations in Arizona and Minnesota. We compared three statistical techniques (Reduced Major Axis regression, Gradient Nearest Neighbor imputation, and Random Forests regression trees) for modeling biomass to better understand how the choice of model type affected predictions of biomass dynamics. Models from each technique were applied across the 20+ year Landsat time-series to derive biomass trajectories, to which a curve-fitting algorithm was applied to leverage the temporal information contained within the time-series itself and to minimize error associated with exogenous effects such as biomass measurements, phenology, sun angle, and other sources. The effect of curve-fitting was an improvement in predictions of biomass change when validated against observed biomass change from repeat FIA inventories. Maps of biomass dynamics were integrated with maps depicting the location and timing of forest disturbance and regrowth to assess the biomass consequences of these processes over large areas and long time frames. The application of these techniques to a large sample of Landsat scenes across North America will facilitate spatial and temporal estimation of biomass dynamics associated with forest disturbance and regrowth, and aid in national-level estimates of biomass change in support of the North American Carbon Program.

1. Introduction

Quantifying the variability of forest biomass over large spatial extents and long time periods is critical for accurate carbon accounting (Goetz et al., 2009; Houghton, 2005). Forest biomass dynamics are governed in large part by disturbance and subsequent regrowth processes (Harmon et al., 1990; Wofsy & Harris, 2002). Inventory-based carbon accounting approaches (e.g. Woodbury et al., 2007) are constrained by the spatial and temporal frequency of sampling, as well as the distribution of samples, and hence might not adequately capture disturbance processes (Houghton, 2005). For regional- to global-scale carbon accounting, this means that maps of disturbance and regrowth, and related biomass and biomass change, are needed across large areas for as long a time frame as possible (Pacala et al., 2007). Satellite imagery and field data (in combination with ecosystem process models) are essential requirements for this purpose (Cohen et al., 1996; Potter et al., 2008). Carbon accounting studies that fail to consider where on a landscape and at what rate forests are disturbed might fail to capture the true spatial and temporal heterogeneity of carbon stocks and flux. Masek and Collatz (2006) demonstrated that for a heavily managed forest area in central Virginia, interannual variability in rates of forest disturbance accounted for approximately one-quarter of the modeled net ecosystem productivity (NEP) variability. This underscores the importance of both stand age and biomass on governing the stocks and fluxes of carbon in forest ecosystems. This paper focuses on the linkage between field measurements and satellite remote sensing to map live aboveground forest biomass and biomass change at broad spatial scales within the United States.

For the satellite component of a global biomass mapping system, the National Academy of Sciences recommended to NASA that they build a mission specifically designed to measure and map biomass and

* Corresponding author. Tel.: +1 406 994 5017.
E-mail address: spowell@montana.edu (S.L. Powell).

0034-4257/$ – see front matter © 2009 Elsevier Inc. All rights reserved.
doi:10.1016/j.rse.2009.12.018

biomass change. This mission, called Deformation, Ecosystem Structure and Dynamics of Ice (DESDynI) is currently in the design phase and will consist of a radar mapping sensor paired with a lidar sampling sensor. The advantages of these sensors include transparency to atmospheric moisture (radar), which is particularly important in tropical and boreal systems, and high sensitivity to biomass change (lidar) (Drake et al., 2002; Lefsky et al., 2002, 2001). In combination with other spatial datasets, including those from existing remote sensing satellites, data from this new mission will facilitate more accurate measurements of biomass dynamics than are currently possible. However, the urgency of climate change means that we cannot afford to wait until 2017, the approximate expected launch date for DESDynI, to begin the work of mapping regional to continental forest biomass dynamics.

In advance of the DESDynI mission, we must rely on existing satellite data. Moreover, because of the critical importance for carbon accounting of recent trends in forest biomass dynamics (Houghton, 2005), a satellite program having a relatively long historical record is important. Additionally, as forests are generally managed at a grain size significantly less than 1000 m (Cohen et al., 2002; Healey et al. 2008; Townshend & Justice, 1980), relatively fine-grained satellite data are needed. Landsat is the only satellite program that has these critical specifications. Landsat has the longest data record (since 1972), a spatial resolution in accordance with the grain of land management (30 m), and a long history of widespread use and acceptance (Cohen & Goward, 2004). Now that the global archive of Landsat data at the USGS is being made available for free in a standard processing format (Woodcock et al., 2008), it is becoming practical to use Landsat data to map recent forest disturbance and regrowth processes over large areas of the earth (Goward et al., 2008). This is particularly true for the United States, which has the greatest spatio-temporal density of Landsat acquisitions in the USGS archive (Goward et al., 2006).

For the field data component globally, we must rely on existing and newly acquired datasets (Cihlar et al., 2002). In the United States, the Forest Inventory and Analysis (FIA) Program of the US Forest Service has for many decades been collecting field measurements that can be used to calculate aboveground forest biomass (Bechtold & Scott, 2005; Jenkins et al., 2003). Linking the FIA field data-derived biomass measurements and the Landsat spectral data via modeling facilitates the mapping of forest biomass and biomass change. Several approaches to linking field measurements and spectral data to map forest characteristics are possible. Two common approaches are radiant transfer models (Hall et al., 1995; Myneni et al., 1997) and empirical models (Cohen et al., 2003; Healey et al., 2006).

In this study, our main goal was to demonstrate an approach for deriving and validating Landsat-based maps of biomass and biomass change over approximately 20 years. Within that goal, there are three objectives: (1) compare and contrast examples of three empirical modeling approaches for mapping biomass (linear regression, imputation, and regression trees); (2) use the Landsat image time-series to leverage the temporal information contained in the spectral signals to more accurately map biomass and its dynamics; and (3) integrate derived biomass and biomass change maps with maps of forest disturbance and regrowth. This last objective demonstrates a unique application of biomass modeling that provides a contextual framework for interpretation of biomass dynamics relative to disturbance processes.

1.1. Empirical modeling of biomass as a static variable

The limitations to empirical modeling of biomass using a single date of passive, optical remote sensing data are well known, most notably the problem of data saturation at high biomass and leaf area index levels (Steininger, 2000; Turner et al., 1999). These limitations have been borne out over a wide variety of statistical studies using an array of predictor variables (Labrecque et al., 2006; Lu, 2006; Moisen & Frescino, 2002). The benefits of using Landsat data for large area biomass dynamics mapping spanning multiple decades, however, will continue to outweigh these limitations. Here, we briefly review prior biomass modeling applications from each of the three model types we test in this paper: regression, imputation, and regression trees.

Regression approaches have been widely applied for prediction of aboveground forest biomass (Hall et al., 2006; Jakubauskas & Price, 1997; Lefsky et al., 2001; Rahman et al., 2008; Zheng et al., 2004). Labrecque et al. (2006) used polynomial and multiple linear regressions of raw Landsat bands and derived vegetation indices to predict aboveground biomass in Newfoundland, Canada. They found that for a single regression equation for all forested areas, the model that explained the most variation was the one that incorporated only the raw Landsat bands. For three study sites, Foody et al. (2003) found that multiple regressions with raw Landsat TM bands explained at least as much, and generally more of the variation in tropical forest biomass as did derived vegetation indices. In Yellowstone National Park, Jakubauskas and Price (1997) found that multiple regression models of biomass from derived spectral indices did not greatly improve predictions of aboveground biomass over models using only raw Landsat TM bands. In contrast, many studies have demonstrated that the inclusion of derived spectral indices and biophysical variables, in addition to raw spectral bands, can improve biomass predictions. Hall et al. (2006) used Landsat ETM + data to model aboveground biomass in Alberta, Canada, and found that the additions of modeled stand height and crown closure as predictor variables significantly improved model error over spectral-only models. Similarly, Zheng et al. (2004) augmented spectral-only modeling of aboveground biomass using stand age as a predictor variable in Wisconsin. In our study, we tested a variation of linear regression called Reduced Major Axis (RMA) regression, an orthogonal regression technique that minimizes error in both the X and Y directions (Larsson, 1993). RMA regression has been shown to be more effective than ordinary least-squares (OLS) regression at maintaining the data variance structure by reducing the attenuation and amplification of predictions at the high and low ends of the observed range, respectively (Cohen et al., 2003). Recent applications of RMA in remote sensing include a diversity of efforts to predict forest structural attributes such as percent cover (Powell et al., 2008b; Schroeder et al., 2007), basal area (Healey et al., 2006), and leaf area index (LAI) (Berterretche et al., 2005).

Non-parametric imputation approaches are widely used for forest inventory mapping applications (Franco-Lopez et al., 2001; Tomppo et al., 2009). These approaches have the ability to map large assemblages of response variables, thereby maintaining the covariance structure of the predicted variables (Ohmann & Gregory, 2002). Labrecque et al. (2006) used the k-NN method with five neighbors and two different weighting functions to estimate aboveground biomass in Newfoundland. For both functions, they found similar accuracies to the multiple linear regression approach mentioned above. In Sweden, Fazakas et al. (1999) used a k-NN approach to model tree biomass using raw Landsat TM bands, and found that the RMSE was inversely related to the scale of the validation data. In our study, we applied Gradient Nearest Neighbor (GNN) imputation using a single neighbor ($k=1$) and its associated attribute, in this case aboveground biomass, to each unmapped pixel based upon a multivariate distance in predictor variable gradient space. In contrast to a regression approach, GNN assigns an actual observed biomass plot value to each “prediction”. In one application of GNN, Ohmann and Gregory (2002) found that ancillary biophysical data, such as elevation and climate data, can aid in the prediction of vegetation variables across large study areas with strong biophysical gradients. In another application, Pierce et al. (2009) found that GNN was accurate for predicting large groups of forest structural attributes at the regional scale and maintaining covariance among the response variables.

Non-parametric regression tree methods have begun to receive considerable attention for prediction of forest structural attributes (Hansen et al., 2002) and for ecological applications in general (Cutler et al., 2007; Lawrence et al., 2006), in part because they have tremendous analytical and operational flexibility. Blackard et al. (2008) used a regression tree approach to develop a national aboveground biomass map using MODIS imagery and ancillary data for the conterminous U.S. Moisen and Frescino (2002) compared regression tree models with several other statistical techniques for prediction of biomass across five ecoregions in the interior western U. S. In our study we used Random Forests (RF) implemented through the R package ModelMap (Freeman & Frescino, 2009). RF is a non-parametric ensemble modeling approach that constructs numerous small regression trees that vote on predictions, and is considered to be robust to over-fitting (Breiman, 2001). Several recent studies have demonstrated the utility of RF for prediction of forest attributes, including successional stage (Falkowski et al., 2009), tree species distribution (Prasad et al., 2006), and tree crown damage resulting from fire (Thompson & Spies, 2009).

From these diverse studies, we know there is little consensus on which statistical method or set of predictor variables is the most robust across a range of forest conditions (Lu, 2006). This is not surprising, as empirical methods commonly draw upon somewhat idiosyncratic statistical relationships associated with model type, forest system under study, and variables derived or available for parameterization. Moreover, for any given modeling scenario there are a host of exogenous effects not related to any inherent relationship between spectral response and biomass that influence the statistical fit of that relationship. These include the atmosphere, sun angle, phenological state of vegetation at the time of image acquisition, topography, and imperfections in radiometric calibration and geometric registration. Here, we demonstrate how temporal fitting of biomass predictions through a time-series mitigates some of the "noise" associated with these exogenous effects.

1.2. Temporal fitting of biomass trajectories

The growing availability of historical Landsat data introduces the possibility of routinely using temporal context to improve prediction of biophysical variables such as biomass. One approach that leverages temporal information involves smoothing a time-series of predictions at the pixel level. Such temporal smoothing may be advantageous in two important ways. First, doing so may improve estimates of biomass change, compared to the more commonly applied two-date change-detection method. Second, improved predictions of biomass at any given point along the time-series may be possible.

Shown in Fig. 1 are two examples of temporal biomass trajectories. Clearly evident is the temporally unstable nature of biomass predictions derived from the linkage of field data and Landsat spectral data (these methods are described in the next section). For the clearcut example, we see a slowly rising multi-year trend that, in its raw form, has a high temporal frequency of increase followed by decrease. Near the end of the time-series (2001–2003) is a precipitous drop in biomass as a result of harvest. A fitting algorithm described by Kennedy et al. (2007; in review) tracks the temporal development of biomass at the pixel level, ignoring the high-frequency variation associated with exogenous factors. The second example shows temporal regrowth after harvest that, although noisy in terms of biomass predictions, is fitted by the smoothing algorithm to depict a more realistic temporal trend in biomass accumulation (1985–2005).

Little is known about how the type of statistical model or choice of predictor variables affects the prediction of biomass trajectories. Few, if any, studies have specifically examined empirical techniques for predicting change in aboveground forest biomass over large areas and long time intervals using temporal trajectories. However, several related studies focusing on percent tree cover (Schroeder et al., 2007),

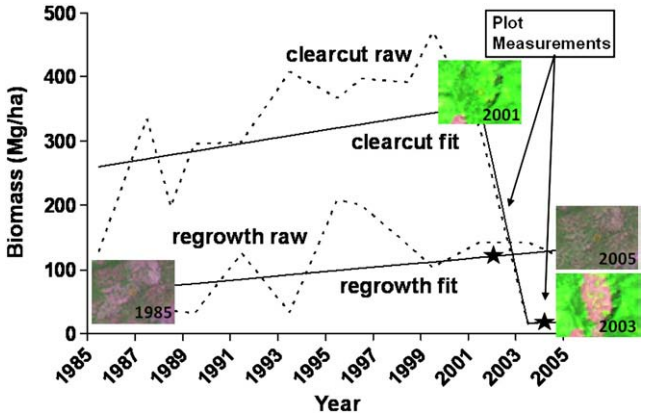

Fig. 1. Example biomass trajectories demonstrating the effect of curve-fitting (solid lines) on raw biomass predictions (dashed lines) for two recently disturbed plots. Landsat image chips centered on the plots are shown along with corresponding plot-level biomass observations.

basal area (Healey et al., 2006), and impervious surface (Powell et al., 2008a) have demonstrated some of the advantages of using Landsat time-series data. Foremost is the ability to examine temporal trends, which is facilitated by the application of a single empirical model across a normalized, consistent time-series of spectral data. Trend analysis offers greater confidence in predictions than single-date assessment or two-date change analysis by minimizing error associated with the aforementioned exogenous factors such as solar angle, phenology, or atmospheric conditions.

1.3. Integration of biomass maps with maps of disturbance

An important application of this work to map biomass and biomass change is to quantify the biomass consequences of forest disturbance and regrowth over approximately 50 Landsat scenes in the U.S (Fig. 2). This is part of a larger study, called North American Forest Dynamics (NAFD) (Goward et al., 2008; Huang et al., 2009, 2010), that is integral to the North American Carbon Program (NACP), within which derived maps of forest dynamics will be linked to ecosystem process models to quantify carbon dynamics across the conterminous U.S (Masek & Collatz, 2006). In this study, forest disturbances are identified by way of an algorithm called Vegetation Change Tracker (VCT) that quantifies abrupt spectral changes in forested pixels and labels the year that the likely disturbance occurred (Huang et al., 2010). Independent validation across a wide variety of forest types indicates a level of accuracy exceeding 80% (Huang et al., 2010).

An important advantage of linking the results of these two studies is that by accurately identifying the locations and timing of disturbances with the VCT, we can then quantify the biomass consequences of disturbance and regrowth processes. This linkage focuses the analysis of biomass dynamics on the most important and uncertain places on the landscape from a carbon modeling perspective. Moreover, in these locations, the change in spectral reflectance is greatest, and hence the change in biomass signal-to-noise ratio is the greatest (both in terms of the disturbance event and the subsequent regrowth). Other notable biomass modeling efforts have produced national-level maps of biomass (Blackard et al., 2008; Kellndorfer et al., 2004) which help contribute to estimates of uncertainty in carbon accounting. Like our effort, both of these faced similar issues with data saturation at high biomass levels. Unlike our effort, however, these studies only provided snapshots of biomass at a single point in time. The unique contributions of our work are the temporal component and the linkage with disturbance mapping. Biennial estimates of changes in biomass stocks in relation to forest disturbance and regrowth will enable us to quantify how much biomass existed in forests prior to disturbance, how much biomass was potentially

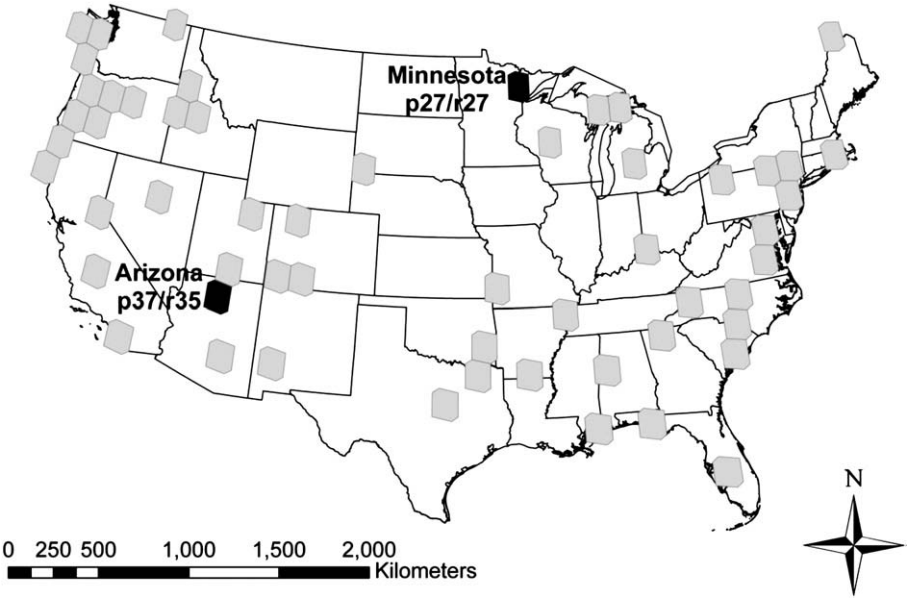

Fig. 2. Arizona (Landsat path 37/row 35) and Minnesota (Landsat path 27/row 27) study scenes (in black) along with the full North American Forest Dynamics sample of over 50 Landsat scenes (in gray) within the conterminous United States of America.

affected as a result of disturbance, and the variable rates of biomass regrowth following disturbance. Whether disturbances occurred in "average" forests with respect to biomass remains a key area of uncertainty for carbon modeling (Houghton, 2005).

2. Methods

2.1. Study areas

We selected two Landsat scenes for analysis, representing markedly different forest types, disturbance regimes, and biophysical settings (Fig. 2). The first study scene, in northern Arizona (Landsat path 37/row 35) encompasses parts of the Grand Canyon region, and has strong environmental gradients, with high elevation mesic coniferous forests transitioning to low elevation xeric coniferous forests and woodlands. Elevations range from less than 600 m along the Colorado River to over 3800 m in the San Francisco Peaks near Flagstaff, Arizona. Because of this mountainous terrain, average annual precipitation and temperature vary widely, between approximately 15–88 cm and minus 5–20 °C, respectively (Thornton et al., 1997). Fire and logging have strongly shaped the age distribution and composition of the nearly 1 million hectares of forest in this study scene. Between 1986 and 2006, the annual rate of forest disturbance varied between less than 0.1 and 2.8% of the total forest area (Huang et al., 2010). The second study scene, in northern Minnesota (Landsat path 27/row 27) spans the region between Lake Superior and the Boundary Waters, and has less pronounced environmental gradients than the Arizona scene. Elevations range from 174–634 m. Average annual precipitation is generally higher in this scene, but has a narrower range between 49 and 109 cm (Thornton et al., 1997). Average annual temperature ranges between approximately 1–7 °C (Thornton et al., 1997). The nearly two and a half million hectares of forest in the Minnesota scene are composed of mixed deciduous and coniferous forests, and contain large areas of woody wetlands. Between 1985 and 2006, the annual rate of forest disturbance in the scene varied between 0.5 and 1.7% of the total forest area (Huang et al., 2010), mostly related to forest harvest, suburbanization, and wind storms. The scene contains a large portion of the 1999 Boundary Waters–Canadian derecho (wind storm) that leveled approximately 27,000 ha of forest in the study area (Nelson et al., 2009).

2.2. Landsat data development

We acquired approximately biennial Landsat time-series stacks between ca. 1985 and ca. 2006 for both sample scenes (Table 1). The best quality, cloud-free images were acquired for each scene as close to peak growing season anniversary dates as possible to minimize the effects of vegetation phenology, sun angle differences, and other exogenous factors. The image data were ortho-corrected (28.5 m resolution) and radiometrically calibrated to surface reflectance with the Landsat Ecosystem Disturbance Adaptive Processing System (LEDAPS) algorithm (Masek et al, 2006). Each image was then radiometrically normalized to a common reference image (noted in Table 1) using the Multivariate Alteration Detection (MAD) method (Canty et al., 2004, Schroeder et al., 2006) to further minimize unimportant temporal spectral variability. Clouds and cloud shadows were not explicitly masked from the Landsat imagery prior to analysis because the temporal biomass fitting algorithm was robust to anomalies associated with clouds and cloud shadows (Kennedy et al., in review).

2.3. FIA data development

Within each Landsat sample scene area, we developed FIA plot-level estimates of live aboveground tree biomass for the most recent

Table 1
Landsat time-series stacks for the two sample scenes, with normalization reference images noted by *.

Arizona	Minnesota
06/21/1985	06/28/1984
07/26/1986	08/21/1986
07/02/1989	09/14/1989
06/19/1990	07/31/1990
06/22/1991	08/19/1991
06/27/1993	08/24/1993
06/14/1994	08/14/1995
06/22/1997	09/04/1997
06/25/1998	08/06/1998
06/14/2000*	07/24/1999
06/12/2002	07/05/2001
07/09/2003	09/05/2003*
08/31/2005	08/06/2004
09/03/2006	09/13/2006

inventory for each state (Table 2) (Bechtold & Scott, 2005). Each FIA plot consists of four 7.3-meter radius subplots, from which we summed per-live tree aboveground biomass for all trees over 1 in. diameter (DRYBIOT variable). We only used plots that represented homogenous (a.k.a. "single condition") forested areas to minimize potential modeling error. This resulted in the exclusion of approximately 22% of forested plots in Arizona and nearly 40% of forested plots in Minnesota. We calculated biomass change for a subset of plots that were remeasured between successive FIA inventories for each study scene (Table 3).

2.4. Empirical modeling

For each FIA plot location, we extracted the mean values from a 3×3 pixel window for each of the spectral and ancillary predictor variables. The Landsat spectral variables were extracted from image dates that closely approximated FIA inventory years. Because of potential spatial and temporal mis-match between the FIA and Landsat data sets, as well as clouds and cloud shadows, a preliminary step in the modeling process was to examine the data for outliers to ensure a high data quality standard. Outliers were identified by creating scatter plots of biomass versus Landsat spectral values and then examining FIA plots that greatly deviated from the expected relationship. For the Arizona and Minnesota scenes, approximately 12% and 8% of FIA plots were identified as outliers, respectively. From the population of single condition forest plots within each sample Landsat scene (AZ Cycle 3 and MN Cycle 12), we randomly divided the data into model (2/3 of the data) and validation (1/3 of the data) sets (Table 2). We developed empirical models of live aboveground tree biomass for each statistical modeling technique using a large suite of available predictor variables, grouped into five distinct categories:

- Raw Landsat bands (B1–B5, B7, as surface reflectance).
- Tasseled Cap indices (brightness (TCB), greenness (TCG), and wetness (TCW)) derived directly from the raw Landsat bands using the reflectance-based transformation (Crist, 1985).
- Spectral indices:
  - normalized difference vegetation index (NDVI):
    - = ((B4−B3)/(B4+B3))
  - Tasseled Cap angle (a new variable presented and tested in this study):
    - = arctan(TCG/TCB)
  - Tasseled Cap distance (Duane et al., in press.):
    - $= \sqrt{TCB^2 + TCG^2}$
  - Tasseled Cap disturbance index (Healey et al., 2005):
    - = ($TCB_r - (TCG_r + TCW_r)$) (where $_r$ denotes rescaled Tasseled Cap indices based upon the mean and standard deviation of the scene's forest values)
- Topographically derived variables, at 28.5 m spatial resolution, including elevation, slope, and a measure of potential relative radiation (Pierce et al., 2005).
- Climate variables (18 year mean annual values) at 1 km spatial resolution, acquired from DAYMET (Thornton et al., 1997), including temperature, precipitation, growing degree days, water vapor pressure, and shortwave radiation.

The preliminary modeling step was to determine an optimal set of predictor variables for each model type and sample scene to compare results across models. Therefore, for each model type and sample scene, we constructed eight *a priori* models based on unique variable permutations (Table 4), and ranked the results based on several measures of prediction accuracy (described in detail below). The *a priori* models were designed to test a hierarchical suite of variable permutations from simple spectral-only models to increasingly complex spectral plus biophysical variable combinations. We used stepwise regression for each of the RMA models to pare down the number of predictor variables and minimize the potential effects of collinearity among predictor variables. We then used canonical correlation analysis (CCA) to integrate the predictor variables into a single index that was optimally correlated with the biomass response variable. This was demonstrated by Cohen et al. (2003), whereby a simple formulation of RMA requires one response variable and one predictor variable. Similarly, for GNN, a stepwise regression procedure with a variance inflation threshold was used to pare down the predictor variables to produce more parsimonious models. No variable reduction technique was employed for RF. While some RF studies have indeed used variable reduction techniques for achieving more parsimonious models (Falkowski et al., 2009), this non-parametric modeling approach is considered robust to collinearity among predictor variables and, therefore, variable reduction techniques are not commonly applied.

Table 4
A priori variable permutations.

Variable permutations
Landsat bands
Landsat bands + spectral indices
Landsat bands + spectral indices + topographic variables
Landsat bands + spectral indices + topographic variables + climate variables
Tasseled Cap indices
Tasseled Cap indices + spectral indices
Tasseled Cap indices + spectral indices + topographic variables
Tasseled Cap indices + spectral indices + topographic variables + climate variables

Table 2
Summary of field measurement years, inventory type, number of plots, and biomass summary statistics for FIA data used for model building and validation for both study scenes.

State	Meas. years	Inventory type	# Plots	Mean biomass (Mg/ha)	Std. Dev. biomass (Mg/ha)	Min biomass (Mg/ha)	Max biomass (Mg/ha)
AZ	2001–2004	Annual cycle 3 model building	91	46	61	0	320
AZ	2001–2004	Annual cycle 3 validation	45	50	55	0	233
MN	1998–2003	Annual cycle 12 model building	645	65	47	0	230
MN	1998–2003	Annual cycle 12 validation	333	62	46	0	216

Table 3
Summary of field measurement years, inventory type, number of plots, and biomass summary statistics for each of the remeasurement FIA inventories used in this study.

State	Meas. years	Inventory type	# Plots	Mean biomass (Mg/ha)	Std. Dev. biomass (Mg/ha)	Min biomass (Mg/ha)	Max biomass (Mg/ha)
AZ	1995	Periodic cycle 2	36	48	49	4	239
	2001–2004	Annual cycle 3	36	54	52	5	233
MN	1998–2003	Annual cycle 12	282	62	48	0	222
	2003–2005	Annual cycle 13	282	54	42	0	214

2.5. Plot-level model validation

Biomass predictions for each model type were validated using the withheld validation data set, in terms of root mean square error (RMSE) between observed and predicted values, variance ratio (VR), and bias. We calculated RMSE as follows where ($\hat{y}_i$) was the predicted biomass on the *i*th plot, and (y_i) the observed biomass on the *i*th plot:

$$RMSE = \sqrt{\frac{1}{n}\sum_{i=1}^{n}(\hat{y}_i - y_i)^2}$$

The variance ratio was calculated as the standard deviation of predicted biomass ($\hat{y}$) divided by the standard deviation of observed biomass (y):

$$variance\ ratio = SD\hat{y} / SDy$$

Bias was calculated as the difference between the mean predicted ($\hat{\bar{y}}$) and the mean observed ($\bar{y}$) biomass:

$$Bias = \hat{\bar{y}} - \bar{y}$$

For each model type and sample scene, the optimal set of predictor variables was determined by ranking the results of the eight *a priori* models based on RMSE, VR, and bias. We summed the ranking of each performance measure to arrive at an overall best permutation for each model type and study scene (Table 5). In the case of ties, the more parsimonious permutation ranked higher.

2.6. Curve-fitting

From each model type and sample scene, biomass prediction surfaces were created by applying the optimal empirical model to each image in the time-series (Healey et al., 2006), creating predicted biomass trajectories for each forested pixel. Forested pixels were identified based on the FIA forest type map (Ruefenacht et al., 2008). These biomass trajectories were then "smoothed" using a set of linear segmentation algorithms, called LandTrendr, based on the work of Kennedy et al. (2007; in review). For each pixel, the yearly time-series of Landsat-derived biomass was modeled as a series of sequential straight-line segments (of arbitrary duration) that captured both abrupt disturbance events and slow accumulation or loss processes while reducing year-to-year noise caused by exogenous factors. The general strategy was to develop a set of increasingly complex models of the trajectory, ranging from one segment spanning the entire period to many segments of arbitrary durations, enabling the possibility of capturing multiple disturbance events within a trajectory. To develop these models, algorithms first identified an initial set of potential vertices (or breakpoints) based on minimizing mean square error or on maximizing directional change between successive segments. The initial set of vertices represented the most complex representation of the trajectory, here limited to seven vertices for the 20+ year period. Vertices were connected using either standard least-squares regression, suitable for trends, or point-to-point connection, suitable for disjunctions between trends, using iterative fitting techniques that evaluated all segments at once. Then, subsequent algorithms iteratively culled one vertex at a time and re-fit the vertices, keeping track of fitting statistics for each successively simpler model. The best trajectory representation was selected to balance minimization of residual error with increased model complexity. Biomass for each year was taken directly from the fitted lines. Although based on straight-line fitting, the approach can approximate a curvilinear biomass response by fitting several sequential straight-line segments of decreasing slope.

For the remeasured FIA plots, the change in biomass between successive inventories was used to validate the predicted biomass change both before and after application of curve-fitting.

2.7. Scene-level model validation

To assess model differences at a broader spatial scale, we developed scene-level biomass trajectories for each of the model types, based upon extrapolation of each model through the Landsat time-series. We compared these biomass trajectories to scene-level FIA data derived from plot-based statistical estimates of live biomass on forestland for Arizona, and live biomass on timberland for Minnesota from successive inventories. We also visually compared maps of aboveground biomass from each of the three modeling techniques to help assess model differences.

3. Results and discussion

3.1. Empirical modeling of biomass as a static variable

The results of the model type comparison underscore the challenges of model validation and comparison. Plot-level validation revealed important, but inconsistent differences between the three model types. For the Minnesota study scene, no single model consistently performed better across the three assessment measures (RMSE, VR, and bias) (Fig. 3). In terms of RMSE, RF performed best, but this was at the expense of variance, for which RMA was superior. Both GNN and RF deflated the observed variance. In terms of bias, all three model types were similarly biased, with RMA and RF being slightly positively biased, and GNN being slightly negatively biased.

For the Arizona study scene, similar inconsistencies were observed. Each accuracy measure favored a different model type (Fig. 4). In terms of RMSE, RF had the lowest error and RMA had the highest error. For VR, RMA inflated the variance while GNN and RF both deflated the variance. GNN most closely preserved the observed

Table 5
A priori variable permutations and actual variables used to construct the best models for each model type and sample scene.

Model type	Arizona	Minnesota
RMA	*Tasseled Cap indices*: Tasseled Cap brightness, Tasseled Cap greenness	*Tasseled Cap indices + spectral indices*: Tasseled Cap greenness, Tasseled Cap wetness, NDVI, Tasseled Cap angle, Tasseled Cap distance, Tasseled Cap disturbance index
GNN	*Tasseled Cap indices*: Tasseled Cap greenness	*Landsat bands + spectral indices + topographic variables + climate variables*: Landsat band 3, slope, growing degree days
RF	*Tasseled Cap indices + spectral indices + topographic variables + climate variables*: Tasseled Cap brightness, Tasseled Cap greenness, Tasseled Cap wetness, NDVI, Tasseled Cap angle, Tasseled Cap distance, elevation, slope, potential relative radiation, temperature, precipitation, growing degree days, water vapor pressure, shortwave radiation	*Landsat bands + spectral indices + topographic variables + climate variables*: Landsat bands 1–5 and band 7 , NDVI, Tasseled Cap angle, Tasseled Cap distance, elevation, slope, potential relative radiation, temperature, precipitation, growing degree days, water vapor pressure, shortwave radiation

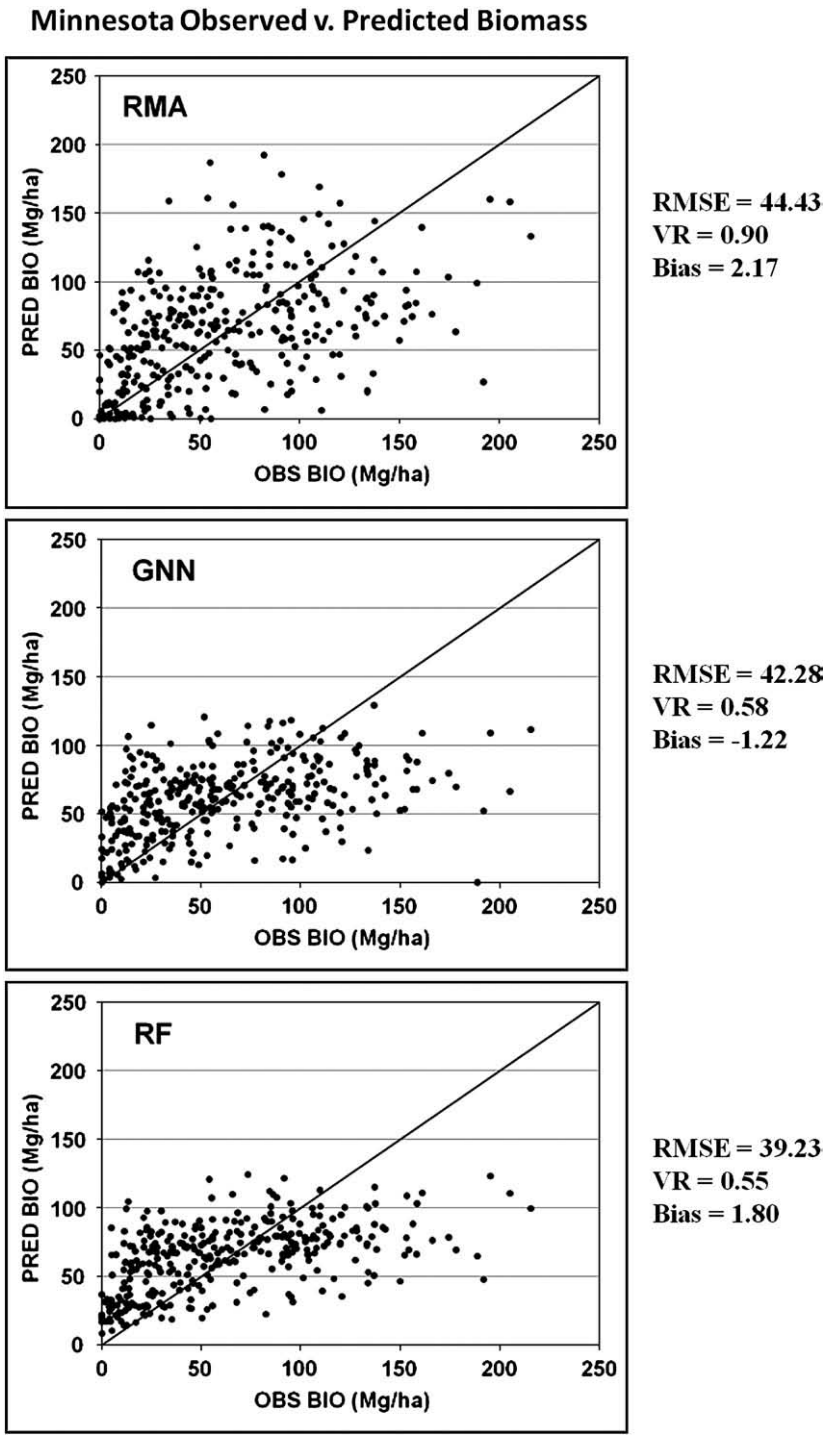

Fig. 3. Observed vs. predicted biomass for each of the three Minnesota models, shown with 1:1 lines.

variance. In terms of bias, all model types produced a negative bias, but RMA was the least negatively biased.

These modeling results are comparable to other studies that have reported plot-level RMSE for modeling aboveground forest biomass. We found that RMSE ranged between 68–87% of the mean observed biomass in Arizona, and between 61–69% in Minnesota. Hall et al. (2006) used regression techniques in Alberta, Canada, and reported an RMSE of 46% of the mean using Landsat bands only. However, they were able to improve the RMSE to 30% by incorporating ancillary biophysical predictors. Fazakas et al. (1999) used a k-NN approach in Sweden and reported a range of RMSE between 72–96% of the mean observed biomass. Labrecque et al. (2006) reported RMSEs of 54% for both regression and k-NN approaches in Newfoundland, Canada.

The differences between the Arizona and Minnesota study scenes help illuminate some key effects of variable inclusion and model type on biomass predictions. The Arizona models generally had lower RMSE than the Minnesota models, and generally tended towards using only a few spectral variables, as opposed to biophysical ones (except in the case of RF). This was likely a result of relatively strong empirical relationships between biomass and the Landsat spectral

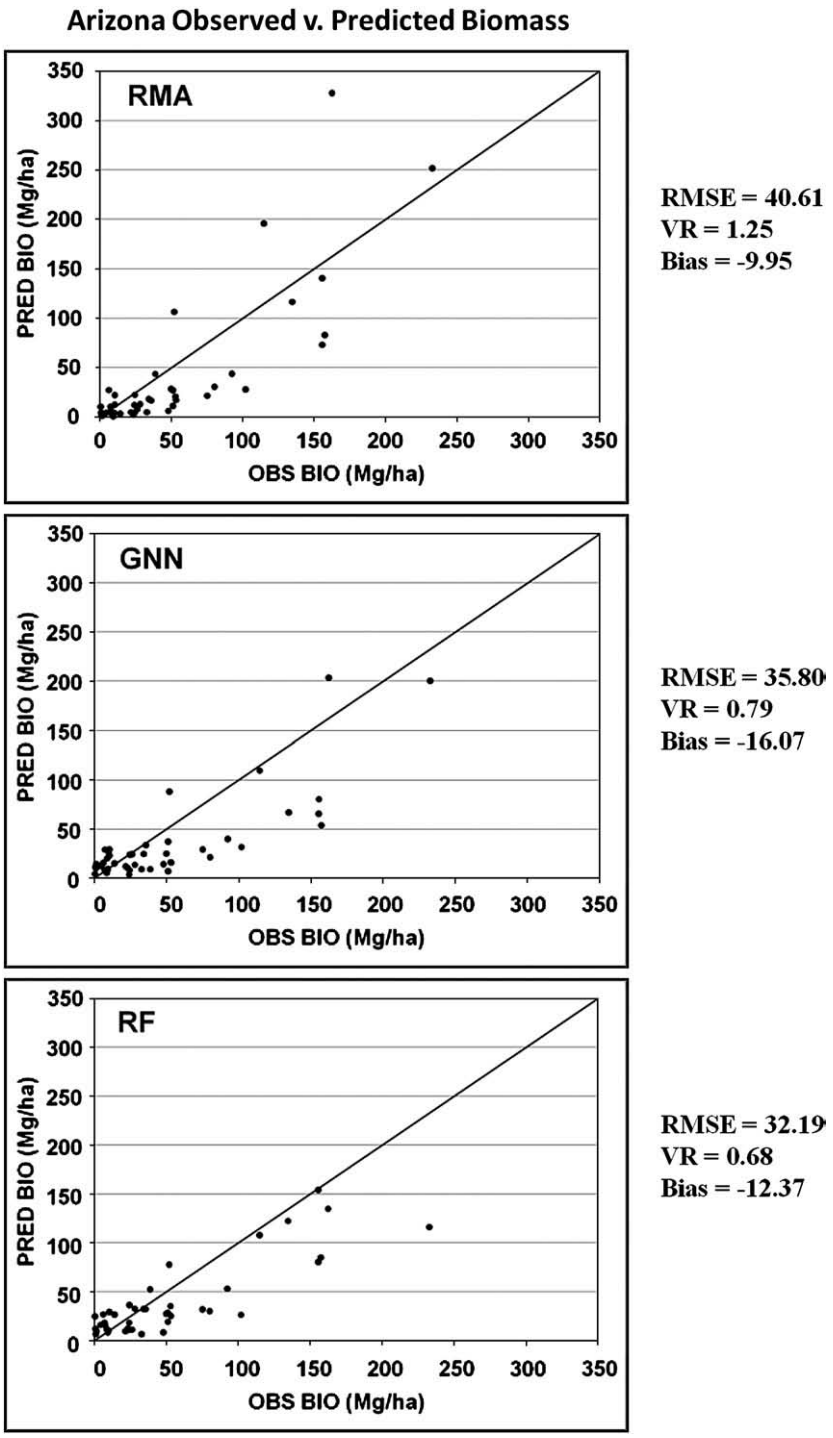

Fig. 4. Observed vs. predicted biomass for each of the three Arizona models, shown with 1:1 lines.

data in this scene. The lowest RMSE in Arizona, however, was achieved with the RF model, which used the most complex set of predictor variables, including both spectral and biophysical ones. The variable importance plot for the Arizona RF model indicated that spectral variables explained the most variability in biomass, but that biophysical variables (including climate variables and elevation) were the second most important set of predictor variables. This result was likely a consequence of strong biophysical gradients in this scene that happened to be correlated with biomass. The higher biomass ponderosa pine forests occur at higher elevations with lower temperatures and higher precipitation. Conversely, the lower biomass pinyon–juniper forests occur at lower elevations with higher temperatures and lower precipitation.

In Minnesota, the results were slightly different. Overall, there was higher RMSE in Minnesota than in Arizona (but also higher mean observed biomass), though there was very little bias across model types. In contrast to Arizona, the models generally required more predictor variables, including biophysical ones, to achieve the best results. This result was likely due to relatively weak empirical relationships between biomass and the Landsat spectral data in this

scene. In addition, there was little correlation between the biophysical variables and biomass. The variable importance plot for the Minnesota RF model indicated that the biophysical variables explained the least amount of variation in biomass. Unlike Arizona, this suggests that patterns of biomass in these forests are more likely related to management, disturbance regimes, or ownership patterns, as opposed to biophysical gradients. We might expect, therefore, that biomass modeling would be more accurate in areas with steep biophysical gradients that are correlated to biomass. We also might expect, given what we know about optical remote sensing data saturation at high biomass levels in different forest types, that biomass modeling would be more accurate in the relatively open canopy, western coniferous forests (with generally steep biophysical gradients), versus the generally closed canopy eastern deciduous forests (also generally lacking in steep biophysical gradients).

As these results and many previous studies confirm, there are significant limitations to empirical modeling of biomass as a static variable using optical remote sensing data. The issue of prediction saturation at high biomass levels, in the absence of stratification, is not easily overcome, though the RMA models do a better job at preserving the observed range of biomass values than RF and GNN. But variance preservation in the case of RMA comes at the expense of overall prediction accuracy, where RF and GNN fare better. Despite relatively high modeling error, we can gain more confidence in our predictions, and attenuate some of the noise associated with exogenous factors by application of these models through a time-series of Landsat observations, and smoothing of the predictions by leveraging the temporal signal.

3.2. Temporal fitting of biomass trajectories

After application of each model through its respective Landsat time-series, we compared the plot-level observed change in biomass from successive FIA inventories to the predicted change in biomass

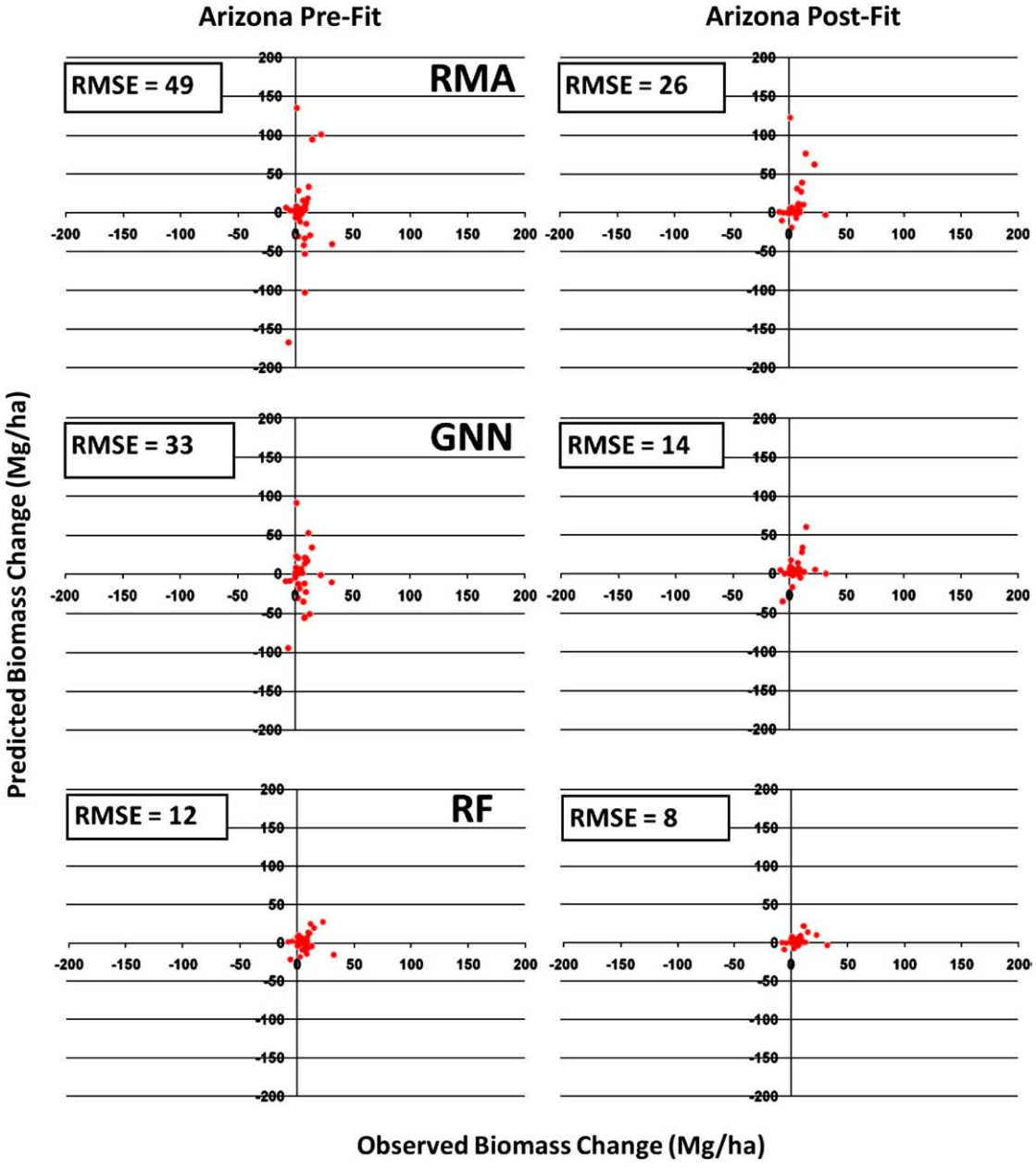

Fig. 5. Arizona observed biomass change vs. predicted biomass change pre- and post-fit by curve-fitting for RMA, GNN, and RF.

both before and after curve-fitting (Figs. 5 and 6). In all cases, the RMSE of predicted biomass change was markedly reduced by curve-fitting. GNN and RMA exhibited the greatest improvements in both Arizona and Minnesota. RF was the most accurate model for predicting biomass change, and hence exhibited the least overall improvement from curve-fitting. All three model types were similarly affected by curve-fitting, with notable compression in the range of biomass change predictions. In Minnesota, this compressed range resulted in under-prediction of biomass affected by disturbance, especially for the GNN and RF models. For example, five observed plots lost at least 100 Mg/ha of biomass due to disturbance between successive FIA inventories, yet predicted losses for those plots from GNN and RF failed to exceed 63 Mg/ha. On the other hand, the RMA model more accurately depicted the range of biomass lost to disturbance, with predicted biomass losses up to 140 Mg/ha. This was a direct consequence of the fact that RMA models inherently do a better job of preserving the observed variance in the predictions. In Arizona, the FIA data did not include observations of significant biomass loss between successive inventories; rather the data contained observations primarily of incremental biomass gains. Here, the RMA model inflated the predictions of biomass increase, likely because the original RMA model over-inflated the predicted variance. Note, however, that erroneous pre-fit predictions of biomass loss were eliminated by curve-fitting, thus greatly improving the RMSE. Likewise for GNN, erroneous predictions of both biomass loss and gain were minimized by curve-fitting. Biomass change predictions from the RF model were the most accurate, both before and after curve-fitting.

Despite relatively high error in predictions of biomass change, curve-fitting clearly represents an improvement over simpler two-date change-detection (akin to the "pre-fit" in Figs. 5 and 6). The inherent modeling problems with biomass as a static variable are not entirely overcome with this approach, but they are mitigated to some extent, namely by exogenous noise reduction among images in the time-series.

Extrapolating to the scene-level, we examined biomass trends across the time-series. Average biomass in the Minnesota scene

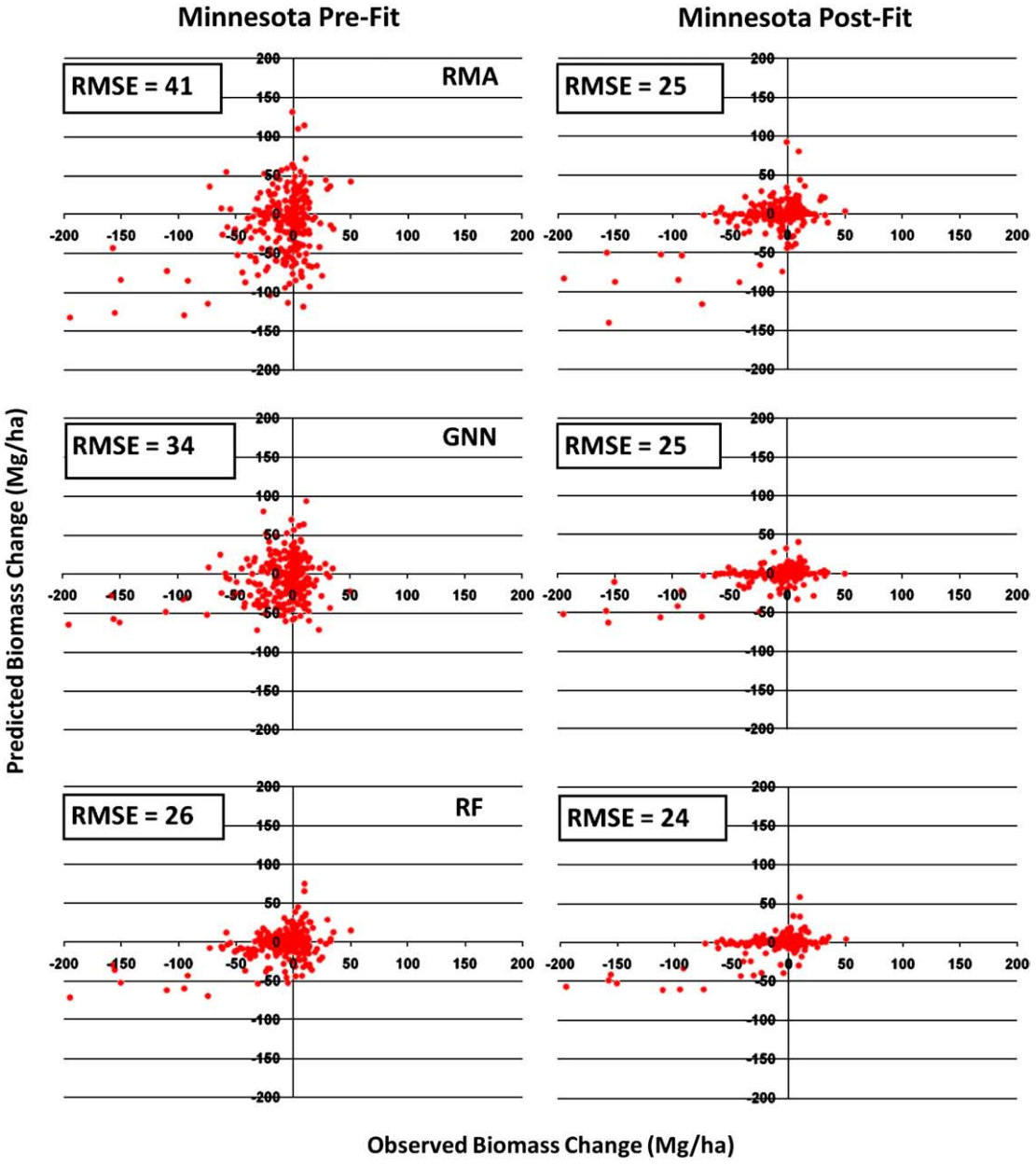

Fig. 6. Minnesota observed biomass change vs. predicted biomass change pre- and post-fit by curve-fitting for RMA, GNN, and RF.

decreased by 5.2% between 1990 and 2003 according to successive FIA inventory data (Fig. 7, top). All three modeled biomass trajectories corroborated this declining trend over that same time period. GNN most closely approximated the observed biomass values at each time period, but underestimated the extent of the decrease (3%). RMA most closely approximated the biomass decline, at 5.4%, but overestimated the observed biomass at both time periods. RF predicted the smallest decline in biomass, only 2.4%.

In Arizona, average biomass increased by 4.9% between 1999–2005 according to the FIA plot-based estimate of biomass change (Fig. 7, bottom). All three modeled biomass trajectories overestimated the observed biomass values at each time period. Both GNN and RF corroborated the observed trend of increasing biomass, but underestimated the extent of the increase. GNN predicted a biomass increase of 0.6% and RF predicted a biomass increase of 0.3%. RMA grossly overestimated the scene-level average biomass and displayed a decreasing biomass trend (17.1%) over that same time period. This was potentially a result of inadequate model training data samples in high biomass hardwood forests that have distinct spectral properties compared to high biomass coniferous forests. Inadequate reference data lead to erroneous linear extrapolation to unrealistically high biomass predictions. This underscores the importance of multiple scales of validation. The plot-based validation of the RMA model failed to demonstrate the significant bias introduced by the scene-level extrapolation of the model. The visual effect of this extrapolation bias can be seen in Fig. 8, which depicts the biomass predictions for each of the model types for a small portion of the Arizona study scene between 1989 and 1990. The RMA predictions for the higher biomass hardwood forests are significantly higher than the corresponding biomass predictions from GNN or RF. At the scene-level, this causes a gross inflation of predicted average biomass and results in erroneous trends. The RMA model relied solely on Tasseled Cap brightness and greenness as predictor variables. The RF model, on the other hand, was robust to the lack of reference data for these rare forests because of its ability to identify complex non-parametric relationships among a broad set of spectral and biophysical variables. The GNN model was

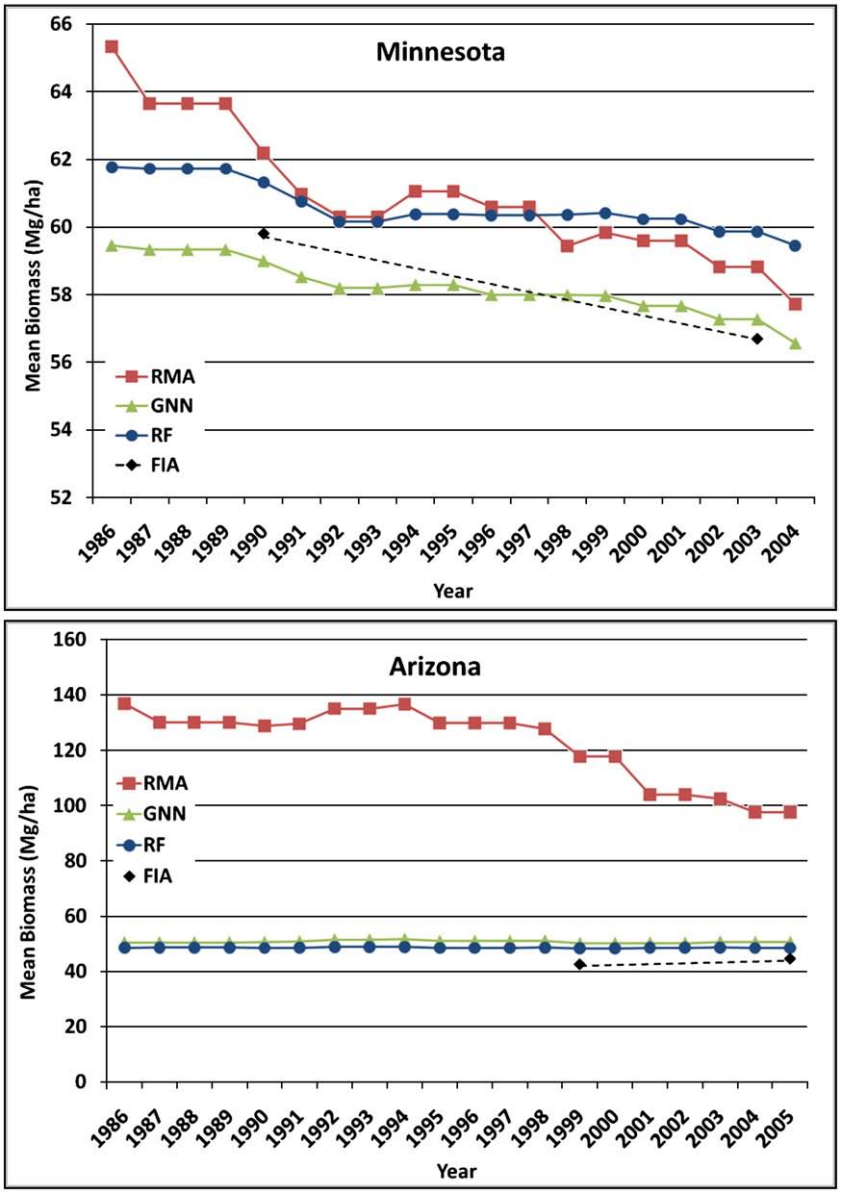

Fig. 7. Scene-level biomass trajectories by model type for Minnesota (top) and Arizona (bottom), with FIA plot-based estimates shown for available years.

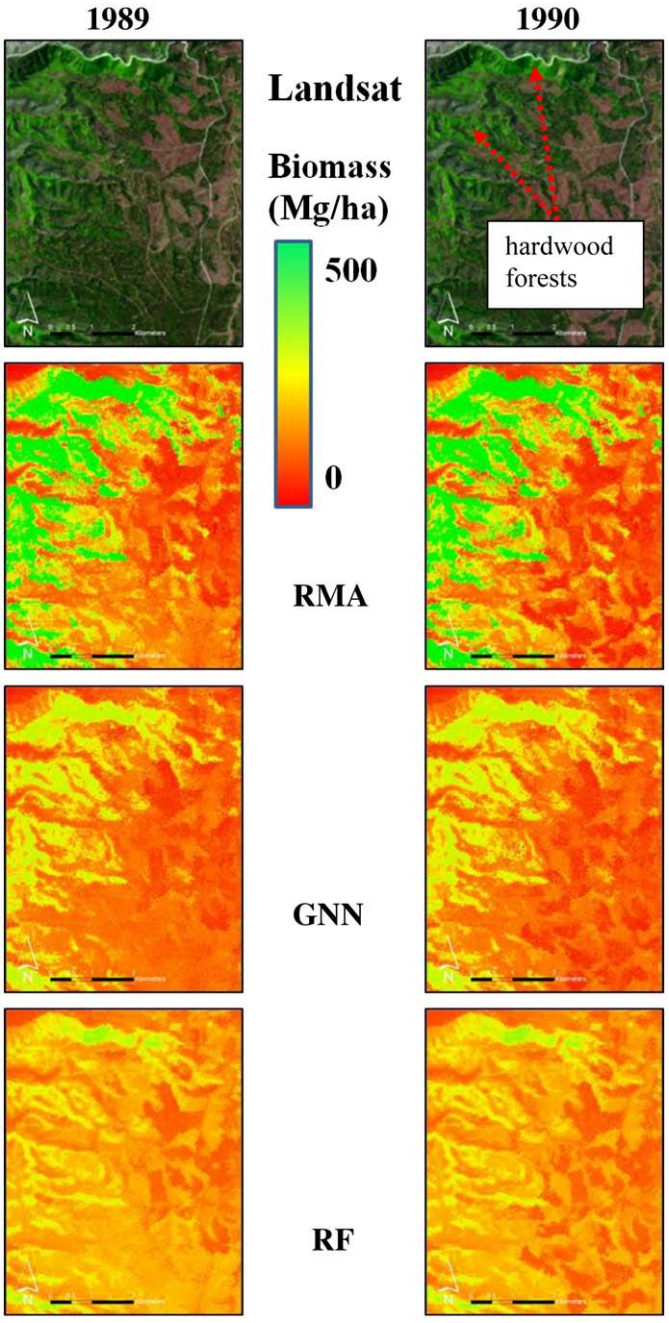

Fig. 8. Visual comparison of mapped model outputs for 1989 and 1990 for a small portion of Arizona. Top panels are Landsat reflectance imagery. The brightest green areas in the Landsat imagery represent hardwood forest.

similarly robust to the lack of reference data, but for different reasons. Imputation methods by design assign an actual response value to each prediction and thus the predictions are restricted to the range of the response variable.

3.3. Integration of biomass maps with maps of disturbance

The results of the related forest disturbance and regrowth study (Goward et al. 2008; Huang et al., 2010) provide a logical framework for analysis of biomass dynamics (Fig. 2). By integrating the results of the two studies we can quantify the consequences of forest disturbance and regrowth on aboveground biomass. More specifically, we can estimate the amount of biomass prior to disturbance, the amount of biomass affected by disturbance, and the rate of biomass regrowth following disturbance. For example, Fig. 9 depicts the trend in area disturbed in Minnesota (Huang et al., 2010) and the aboveground biomass decrease associated with disturbed areas. Both the area disturbed and the biomass decrease spike in 1999 as a result of the Boundary Waters–Canadian derecho event that leveled nearly 27,000 ha of forest in the study area (Nelson et al., 2009). Across the entire study area, we estimated that over 40,000 ha of forest was disturbed during that time period, including the derecho, resulting in nearly 12 Tg of live aboveground biomass loss. In comparison to a more widely known disturbance event, Chambers et al. (2007) estimated that tree mortality associated with Hurricane Katrina in 2005 caused a biomass decrease on the order of 105 Tg of carbon (equivalent to approximately 210 Tg of biomass). Fig. 9 also depicts a significant spike in area disturbed in 2004 with a much smaller associated spike in the amount of biomass decrease. This divergence is likely a result of elevated VCT error in that time period associated with drought, wetland changes, clouds, and false-positive change detection (Thomas et al, in review). Fig. 10 depicts examples from two notable disturbance intervals in the Minnesota study area, including the 1999 derecho event as well as forest harvest between 1990 and 1991. Disturbance maps, biomass predictions, and Landsat imagery before and after the disturbance events are shown for visual examples of the mapped output.

A second example from Arizona illustrates the spatial variability in forest disturbance and the consequences of that variability for aboveground biomass dynamics. Fig. 11 demonstrates that the trend in area disturbed closely corresponds to the trend in biomass decrease, except for a couple of notable anomalies. In one instance, a larger area was disturbed between 1994 and 1997 than between 1998 and 2000, but a lesser amount of biomass was affected. Why would this be the case? An examination of these disturbance intervals revealed that between 1998 and 2000 most disturbances occurred in high biomass ponderosa pine, aspen, and spruce–fir forests and resulted in proportionally large losses of biomass (Fig. 12). In contrast, between 1994 and 1997 most disturbances occurred in lower biomass pinyon–juniper, oak, and ponderosa pine forest and resulted in proportionally smaller losses of biomass. This underscores the importance of deriving spatially explicit maps of biomass dynamics, because the assumption that “average” disturbances occur in “average” forests with respect to biomass may lead to over- or under-estimation of the amount of biomass affected by disturbance, depending upon the nature of the disturbance and the forest.

4. Conclusions

The recently opened Landsat data archive underscores the importance of techniques and applications that leverage the temporal information contained within a time-series of data to improve empirical biomass estimation and quantification of biomass dynamics. While biomass estimation with optical remote sensing data will never be as accurate as estimation by active remote sensing approaches (e.g. lidar and interferometric radar), the immediate need for quantification of biomass dynamics across long time periods and large areas necessitates this type of approach.

There are numerous modeling approaches for empirical estimation of aboveground biomass with spectral and biophysical data. As our results demonstrate, it is difficult to conclude outright that one modeling technique is superior to another. Much depends upon how one prioritizes the different validation measures and scales. In terms of RMSE, RF consistently yielded the best results. Therefore, if minimizing prediction error is the main objective for a study, one might choose to use RF. The same cannot be said for VR, where RF was generally outperformed by RMA and GNN. For some applications, preservation of variance might be important. For example, for

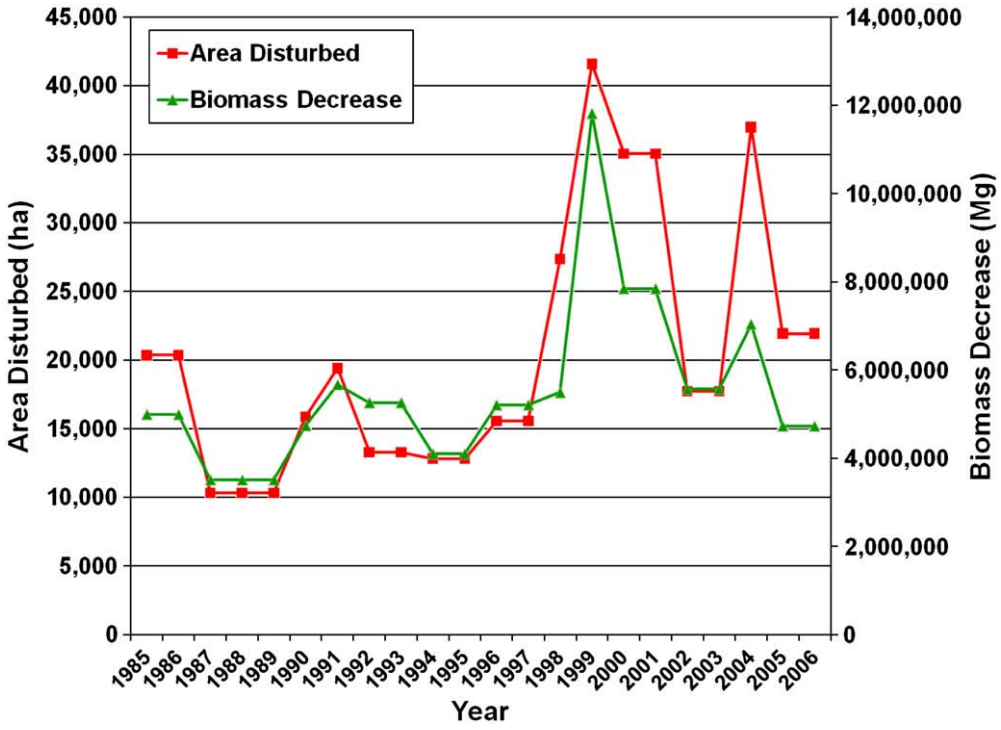

Fig. 9. Minnesota biomass decrease from forest disturbance (from RF model) and area disturbed according to VCT forest disturbance estimates (Huang et al., 2010).

mapping biomass in rare, old-growth forests with extremely high biomass, one might choose to use RMA or GNN for the purposes of variance preservation, as long as adequate training data are available. For other applications, preservation of covariance structure among a suite of predicted forest structural attributes might be of interest, in which case one might choose to use GNN. Of the three plot-level accuracy measures, VR was the most sensitive to the choice of model type. Bias was relatively insensitive to the choice of model type. But plot-level validation is only one aspect of model-type comparisons. Scene-level validation revealed important issues that plot-level validation failed to reveal. For example, inadequate reference data in conjunction with RMA linear model extrapolation caused prediction of unrealistic biomass levels, and hence introduced significant scene-level bias. Analysts may choose a particular modeling strategy based on any number of factors, not the least of which might be the operational ease of implementation. Due to their non-parametric nature, ability to handle various classes of predictor variables, ease of implementation, and relatively low prediction error, RF models are an attractive option.

It is clear from the results of this study that there is significant modeling error that is difficult to overcome at the pixel level. Despite that, the consistency of Landsat observations through time enables us to observe and quantify very real trends in biomass dynamics that we can partially corroborate with various lines of evidence. The key point is that although there is significant modeling error with biomass prediction, the temporal analysis ensures that at least the models are consistent across the time-series, and, therefore, the relative changes are potentially accurate. Linkage with more accurate maps of forest disturbance provides a framework for interpretation of biomass dynamics relative to disturbance and regrowth processes. The temporal application of biomass modeling and the linkage with disturbance mapping represent a unique and powerful contribution of this study.

Further development of the LandTrendr algorithm is ongoing, and future applications will likely employ a modified and improved approach. In this modified approach, LandTrendr will first be used to curve-fit an annual stack of raw spectral data, and then empirical biomass modeling will proceed using the fitted data (Kennedy et al., in review). In contrast to the current approach of curve-fitting biennial biomass predictions, this modified approach can be expected to further minimize temporal variation and more accurately label the timing and magnitude of disturbance and regrowth.

The application of RF models and curve-fitting of biomass trajectories to a large sample of over 50 Landsat time-series across North America will enable a first approximation of continental rates of biomass loss and accumulation as a result of forest disturbance and regrowth (Goward et al., 2008). Despite the known limitations to empirical modeling of biomass with optical remote sensing data, we have demonstrated that by leveraging the temporal data content of a Landsat time-series, we can mitigate some model noise, and roughly quantify long term, large area forest biomass dynamics. These estimates are an important intermediate step, and can provide baseline validation for future satellite missions aimed more specifically at addressing this critical issue.

Acknowledgements

Funding for this study was provided by NASA's Terrestrial Ecology Program. The authors wish to thank Samuel Goward, Chenquan Huang, Nancy Thomas, and Karen Schleeweis of the University of Maryland and Jeff Masek of NASA Goddard for providing the processed time-series data, the disturbance maps, validation results, and guidance along the way. We also wish to thank Tracey Frescino and Elizabeth Freeman of the USDA Forest Service, Rocky Mountain Research Station in Ogden, Utah for providing R programming expertise in the development of code for modeling and mapping with Random Forests. Thanks also to Elizabeth LaPoint of the USDA Forest Service, FIA National Spatial Data Services in Durham, NH, for her invaluable help with many aspects of the FIA data. Finally, the authors wish to thank three anonymous reviewers for their input.

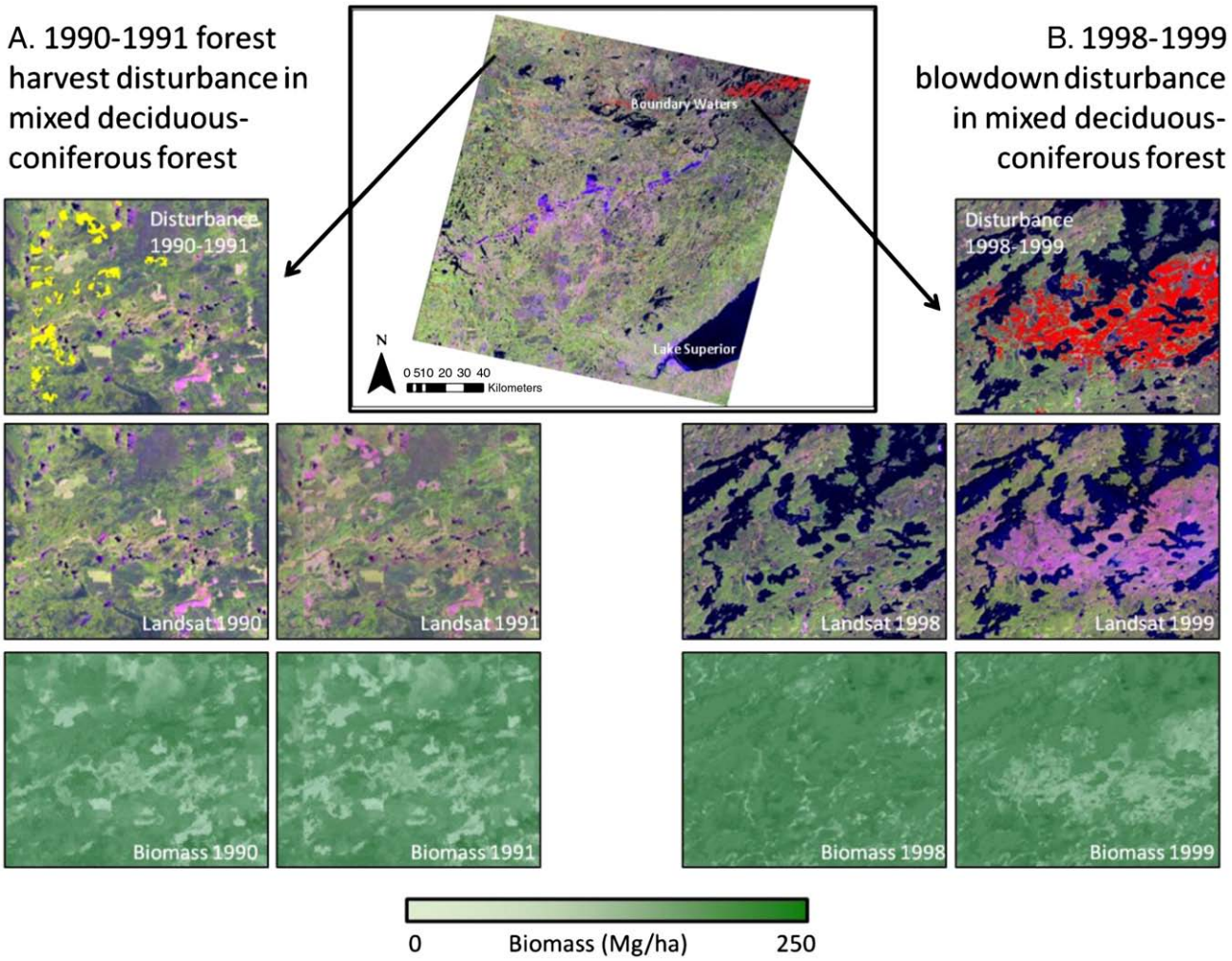

Fig. 10. Example from northern Minnesota (Landsat path 27/row 27) of forest harvest disturbances in mixed deciduous–coniferous forest (yellow) vs. blowdown disturbance in mixed deciduous–coniferous forest (red), shown along with pre- and post-disturbance Landsat imagery and biomass predictions (note: not masked for water, etc...).

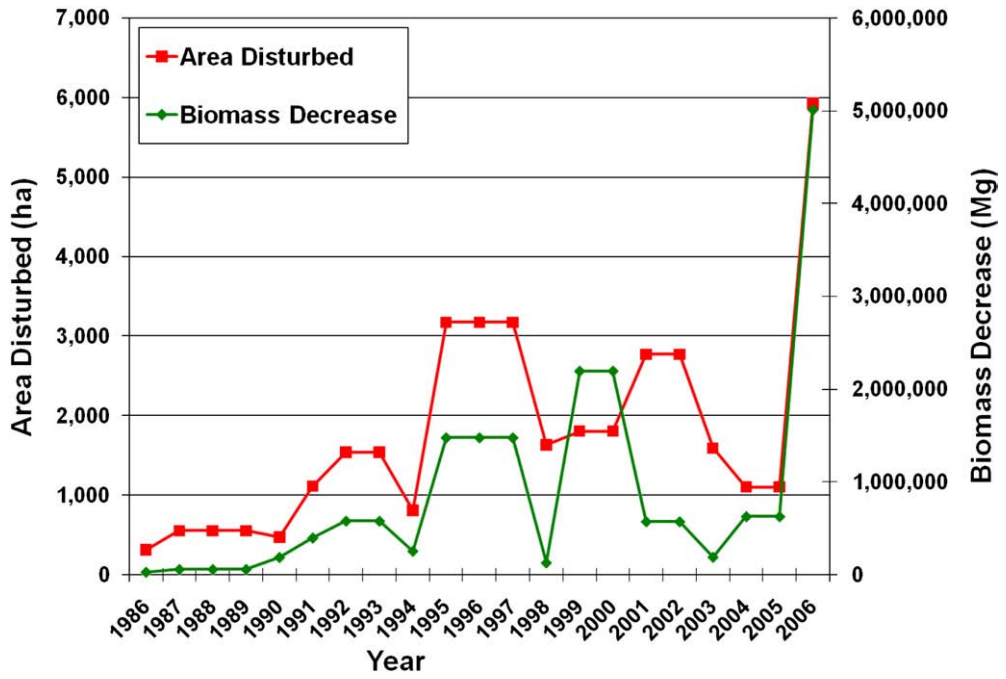

Fig. 11. Arizona biomass decrease from forest disturbance (from RF model) and area disturbed according to VCT forest disturbance estimates (Huang et al., 2010).

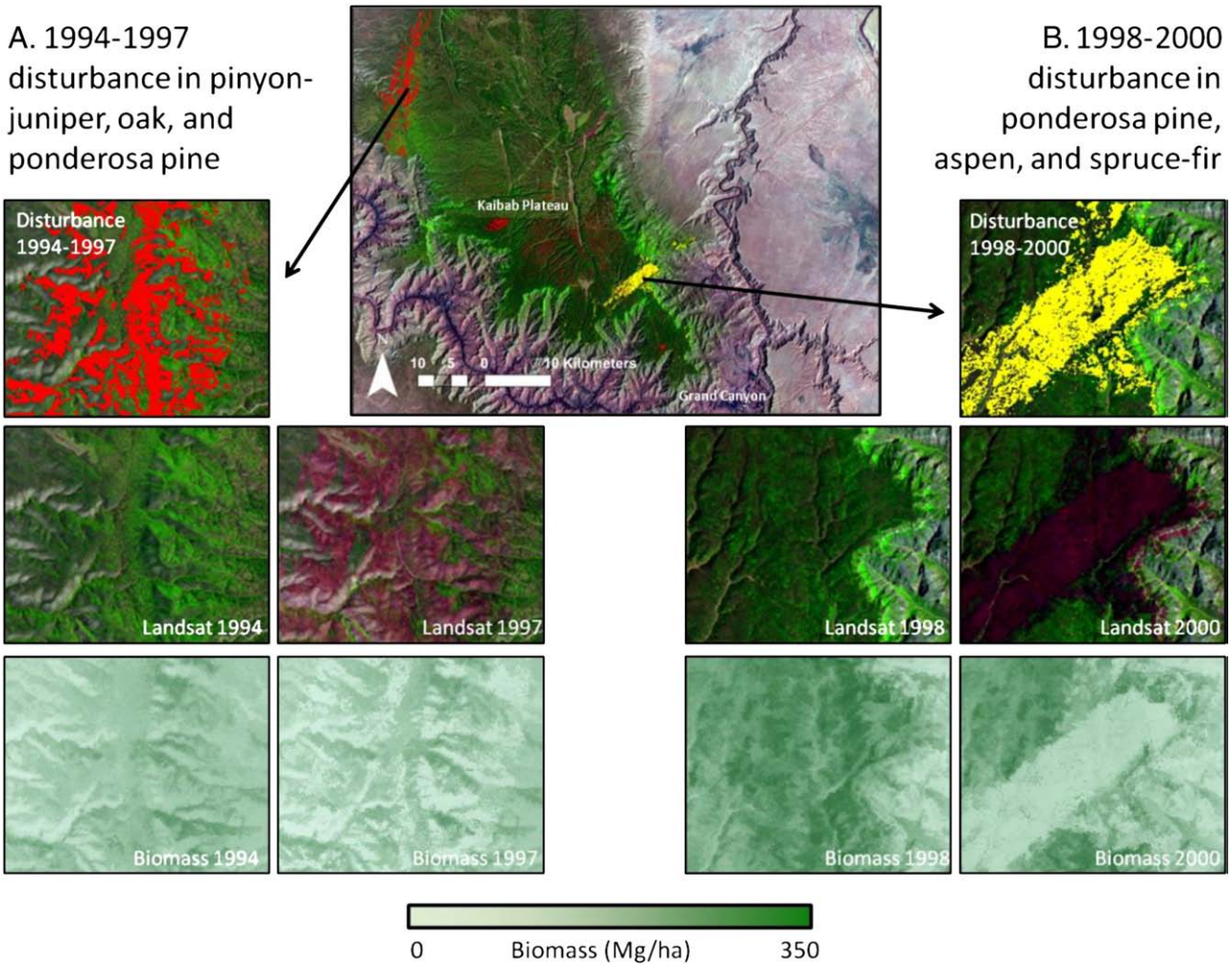

Fig. 12. Example from the Kaibab Plateau, Arizona (Landsat path 37/row 35) of disturbances in higher biomass ponderosa pine forests (yellow) vs. disturbances in lower biomass pinyon–juniper forests (red), shown along with pre- and post-disturbance Landsat imagery and biomass predictions. The difference in pre-disturbance biomass accounts for the divergence seen in Fig. 11 between the moderate amount of area disturbed in the 1998–2000 interval and the relatively high amount of biomass affected during that time period.

References

Bechtold, W. A., & Scott, C. T. (2005). The Forest Inventory and Analysis Plot Design. In W. A. Bechtold, & P. L. Patterson (Eds.), *The enhanced Forest Inventory and Analysis Program—National sampling design and estimation procedures. Gen. Tech. Rep. SRS-80* (pp. 27—42). Asheville, N.C: U.S. Department of Agriculture, Forest Service, Southern Research Station.

Berterretche, M., Hudak, A. T., Cohen, W. B., Maiersperger, T. K., Gower, S. T., & Dungan, J. (2005). Comparison of regression and geostatistical methods for mapping Leaf Area Index (LAI) with Landsat ETM + data over a boreal forest. *Remote Sensing of Environment*, *96*, 49—61.

Blackard, J. A., Finco, M. V., Helmer, E. H., Holden, G. R., Hoppus, M. L., Jacobs, D. M., et al. (2008). Mapping US forest biomass using nationwide forest inventory data and moderate resolution information. *Remote Sensing of Environment*, *112*, 1658—1677.

Breiman, L. (2001). Random forests. *Machine Learning*, *45*, 5—32.

Canty, M. J., Nielson, A. A., & Schmidt, M. (2004). Automatic radiometric normalization of multitemporal satellite imagery. *Remote Sensing of Environment*, *91*(3–4), 441—451.

Chambers, J. Q., Fisher, J. I., Zeng, H., Chapman, E. L., Baker, D. B., & Hurtt, G. C. (2007). Hurricane Katrina's carbon footprint on U.S. Gulf Coast forests. *Science*, *318*, 1107.

Cihlar, J., Heimann, M., Olson, R., Alexandrov, G., Belward, A., Brown, L., et al. (2002). *Terrestrial carbon observation—The Frascati report on in situ carbon data and informationEnvironment and Natural Resources Service Sustainable Development Department*, *vol. 5*,. Rome: Food and Agricultural Organization of the United Nations 120 pp.

Cohen, W. B., & Goward, S. N. (2004). Landsat's role in ecological applications of remote sensing. *BioScience*, *54*, 535—545.

Cohen, W. B., Harmon, M. E., Wallin, D. O., & Fiorella, M. (1996). Two decades of carbon flux from forests of the Pacific Northwest. *Bioscience*, *46*(11), 836—844.

Cohen, W. B., Spies, T. A., Alig, R. J., Oetter, D. R., Maiersperger, T. K., & Fiorella, M. (2002). Characterizing 23 years (1972–1995) of stand replacement disturbance in western Oregon forests with Landsat imagery. *Ecosystems*, *5*, 122—137.

Cohen, W. B., Maiersperger, T. K., Gower, S. T., & Turner, D. P. (2003). An improved strategy for regression of biophysical variables and Landsat ETM + data. *Remote Sensing of Environment*, *84*, 561—571.

Crist, E. P. (1985). A TM tasseled cap equivalent transformation for reflectance factor data. *Remote Sensing of Environment*, *17*, 301—306.

Cutler, D. R., Edwards, T. C., Beard, K. H., Cutler, A., & Hess, K. T. (2007). Random forests for classification in ecology. *Ecology*, *88*, 2783—2792.

Drake, J. B., Dubayah, R. O., Clark, D. B., Knox, R. G., Blair, J. B., Hofton, M. A., et al. (2002). Estimation of tropical forest structural characteristics using large-footprint lidar. *Remote Sensing of Environment*, *79*, 305—319.

Duane, M. V., Cohen, W. B., Campbell, J. L., Hudiburg, T., Turner, D. P., and Weyermann, D. (in press). Implications of alternative field-sampling designs on Landsat-based mapping of stand age and carbon stocks in Oregon forests. Forest Science.

Falkowski, M. J., Evans, J. S., Martinuzzi, S., Gessler, P. E., & Hudak, A. T. (2009). Characterizing forest succession with lidar data: An evaluation for the Inland Northwest, USA. *Remote Sensing of Environment*, *113*, 946—956.

Fazakas, Z., Nilsson, M., & Olsson, H. (1999). Regional forest biomass and wood volume estimation using satellite data and ancillary data. *Agricultural and Forest Meteorology*, *98–99*, 417—425.

Foody, G. M., Boyd, D. S., & Cutler, M. E. J. (2003). Predictive relations of tropical forest biomass from Landsat TM data and their transferability between regions. *Remote Sensing of Environment*, *85*, 463—474.

Franco-Lopez, H., Ek, A. R., & Bauer, M. E. (2001). Estimation and mapping of forest stand density, volume, and cover type using the k-nearest neighbors method. *Remote Sensing of Environment*, *77*, 251—274.

Freeman, E. A. and Frescino, T. A. (2009). ModelMap: An R package for modeling and map production using Random Forest and Stochastic Gradient Boosting. USDA Forest Service, Rocky Mountain Research Station, 507 25th St., Ogden, UT, USA. Eafreeman@fs.fed.us, URL: http://CRAN.R-project.org

Goetz, S. J., Baccini, A., Laporte, N. T., Johns, T., Walker, W., Kellndorfer, J., et al. (2009). Mapping and monitoring carbon stocks with satellite observations: A comparison of methods. *Carbon Balance and Management*, *4*, 2. doi:10.1186/1750-0680-4-2.

Goward, S. N., Arvidson, T., Williams, D., Faundeen, J., Irons, J., & Franks, S. (2006). Historical record of Landsat global coverage: Mission operations, NSLRSDA, and International cooperator stations. *Photogrammetric Engineering and Remote Sensing*, *72*(10), 1155−1169.

Goward, S. N., Masek, J. G., Cohen, W., Moisen, G., Collatz, G. J., Healey, S., et al. (2008). Forest disturbance and North American carbon flux. *EOS*, *89*(11), 105−106.

Hall, F. G., Shimabukuro, Y. E., & Huemmrich, K. F. (1995). Remote-sensing of forest biophysical structure using mixture decomposition and geometric reflectance models. *Ecological Applications*, *5*(4), 993−1013.

Hall, R. J., Skakun, R. S., Arsenault, E. J., & Case, B. S. (2006). Modeling forest stand structure attributes using Landsat ETM + data: Application to mapping of aboveground biomass and stand volume. *Forest Ecology and Management*, *225*, 378−390.

Hansen, M. C., DeFries, R. S., Townshend, J. R. G., Sohlberg, R., Dimiceli, C., & Carroll, M. (2002). Towards an operational MODIS continuous field of percent tree cover algorithm: Examples using AVHRR and MODIS data. *Remote Sensing of Environment*, *83*, 303−319.

Harmon, M. E., Ferrell, W. K., & Franklin, J. F. (1990). Effects on carbon storage of conversion of old-growth forests to young forests. *Science*, *247*(4943), 699−702.

Healey, S. P., Cohen, W. B., Zhiqiang, Y., & Krankina, O. (2005). Comparison of Tasseled Cap-based Landsat data structures for forest disturbance detection. *Remote Sensing of Environment*, *97*, 301−310.

Healey, S. P., Yang, Z., Cohen, W. B., & Pierce, D. J. (2006). Application of two regression-based methods to estimate the effects of partial harvest on forest structure using Landsat data. *Remote Sensing of Environment*, *101*, 115−126.

Healey, S. P., Cohen, W. B., Spies, T. A., Moeur, M., Pflugmacher, D., Whitley, M. G., et al. (2008). The relative impact of harvest and fire upon landscape-level dynamics of older forests: Lessons from the Northwest Forest Plan. *Ecosystems*, *11*(7), 1106−1119.

Houghton, R. A. (2005). Aboveground forest biomass and the global carbon balance. *Global Change Biology*, *11*, 945−958.

Huang, C., Goward, S. N., Masek, J. G., Gao, F., Vermote, E. F., Thomas, N., et al. (2009). Development of time series stacks of Landsat images for reconstructing forest disturbance history. *International Journal of Digital Earth*, *2*, 195−218.

Huang, C., Goward, S. N., Masek, J. G., Thomas, N., Zhu, Z., & Vogelmann, J. E. (2010). An automated approach for reconstructing recent forest disturbance history using dense Landsat time series stacks. *Remote Sensing of Environment*, *114*, 183−198.

Jakubauskas, M. E., & Price, K. P. (1997). Empirical relationships between structural and spectral factors of Yellowstone lodgepole pine forests. *Photogrammetric Engineering and Remote Sensing*, *63*, 1375−1381.

Jenkins, J. C., Chojnacky, D. C., Heath, L. S., & Birdsey, R. A. (2003). National-scale biomass equations for United States tree species. *Forest Science*, *49*(1), 12−35.

Kellndorfer, J. M., Walker, W. S., Pierce, L. E., Dobson, M. C., Fites, J., Hunsaker, C., et al. (2004). Vegetation height derivation from Shuttle Radar Topography Mission and National Elevation data sets. *Remote Sensing of Environment*, *93*(3), 339−358.

Kennedy, R. E., Cohen, W. B., & Schroeder, T. A. (2007). Trajectory-based change detection for automated characterization of forest disturbance dynamics. *Remote Sensing of Environment*, *110*, 370−386.

Kennedy, R. E., Yang, Z., and Cohen, W. B. (in review). Detecting trends in disturbance and recovery using yearly Landsat Thematic Mapper stacks: 1. Processing and analysis algorithm. *Remote Sensing of Environment.*

Labrecque, S., Fournier, R. A., Luther, J. E., & Piercey, D. (2006). A comparison of four methods to map biomass from Landsat-TM and inventory data in western Newfoundland. *Forest Ecology and Management*, *226*, 129−144.

Larsson, H. (1993). Linear regression for canopy cover estimation in Acacia woodlands using Landsat-TM, -MSS, and SPOT HRV XS data. *International Journal of Remote Sensing*, *14*, 2129−2136.

Lawrence, R. L., Wood, S. D., & Sheley, R. L. (2006). Mapping invasive plants using hyperspectral imagery and Breiman Cutler classifications (RandomForest). *Remote Sensing of Environment*, *100*, 356−362.

Lefsky, M. A., Cohen, W. B., & Spies, T. A. (2001). An evaluation of alternate remote sensing products for forest inventory, monitoring, and mapping of Douglas-fir forests in western Oregon. *Canadian Journal of Forest Research*, *31*, 78−87.

Lefsky, M. A., Cohen, W. B., Parker, G. G., & Harding, D. J. (2002). Lidar remote sensing for ecosystem studies. *Bioscience*, *52*, 19−30.

Lu, D. (2006). The potential and challenge of remote sensing-based biomass estimation. *International Journal of Remote Sensing*, *27*, 1297−1328.

Masek, J. G., & Collatz, G. J. (2006). Estimating forest carbon fluxes in a disturbed southeastern landscape: Integration of remote sensing, forest inventory, and biogeochemical modeling. *Journal of Geophysical Research*, *111*, G01006. doi: 10.1029/2005JG000062.

Masek, J. G., Vermote, E. F., Saleous, N., Wolfe, R., Hall, F. G., Huemmrich, F., et al. (2006). Landsat surface reflectance data set for North America, 1990–2000. *Geoscience and Remote Sensing Letters*, *3*, 68−72.

Moisen, G. G., & Frescino, T. S. (2002). Comparing five modeling techniques for predicting forest characteristics. *Ecological Modelling*, *157*, 209−225.

Myneni, R. B., Nemani, R. R., & Running, S. W. (1997). Estimation of global leaf area index and absorbed par using radiative transfer models. *IEEE Transactions on Geoscience and Remote Sensing*, *35*(6), 1380−1393.

Nelson, M. D., Healey, S. P., Moser, W. K., & Hansen, M. H. (2009). Combining satellite imagery with forest inventory data to assess damage severity following a major blowdown event in northern Minnesota, USA. *International Journal of Remote Sensing*, *30*, 5089−5108.

Ohmann, J. L., & Gregory, M. J. (2002). Predictive mapping of forest composition and structure with direct gradient analysis and nearest neighbor imputation in coastal Oregon, USA. *Canadian Journal of Forest Research*, *32*, 725−741.

Pacala, S., Birdsey, R. A., Bridgham, S. D., Conant, R. T., Davis, K., & Hales, B. (2007). The North American carbon budget past and present. In A. W. King (Ed.), *The first State of the Carbon Cycle Report (SOCCR)*,Asheville, N.C.: NOAA Natl. Clim. Data Cent.

Pierce, K. B., Lookingbill, T., & Urban, D. L. (2005). A simple method for estimating potential relative radiation (PRR) for landscape-scale vegetation analysis. *Landscape Ecology*, *20*, 137−147.

Pierce, K. B., Jr., Ohmann, J. L., Wimberly, M. C., Gregory, M. J., & Fried, J. S. (2009). Mapping wildland fuels and forest structure for land management: A comparison of nearest neighbor imputation and other methods. *Canadian Journal of Forest Research*, *39*, 1901−1916.

Potter, C., Gross, P., Klooster, S., Fladeland, M., & Genovese, V. (2008). Storage of carbon in U.S. forests predicted from satellite data, ecosystem modeling, and inventory summaries. *Climate Change*, *90*(3), 269−282.

Powell, S. L., Cohen, W. B., Yang, Z., Pierce, J. D., & Alberti, M. (2008). Quantification of impervious surface in the Snohomish Water Resources Inventory Area of Western Washington from 1972–2006. *Remote Sensing of Environment*, *112*, 1895−1908.

Powell, S. L., Hansen, A. J., & Cohen, W. B. (2008). Mapping the extent and distribution of conifer cover increase in the Greater Yellowstone Ecosystem. In A. Dupont, & H. Jacobs (Eds.), *Landscape ecology research trends* (pp. 27−43). Hauppauge, New York: Nova Science Publishers.

Prasad, A. M., Iverson, L. R., & Liaw, A. (2006). Newer classification and regression tree techniques: Bagging and Random Forests for ecological prediction. *Ecosystems*, *9*, 181−199.

Rahman, M. M., Csaplovics, E., & Koch, B. (2008). Satellite estimation of forest carbon using regression models. *International Journal of Remote Sensing*, *29*, 6917−6936.

Ruefenacht, B., Finco, M. V., Nelson, M. D., Czaplewski, R., Helmer, E. H., Blackard, J. A., et al. (2008). Conterminous U.S. and Alaska forest type mapping using Forest Inventory and Analysis data. *Photogrammetric Engineering and Remote Sensing*, *74*, 1379−1389.

Schroeder, T. A., Cohen, W. B., Song, C., Canty, M. J., & Yang, Z. (2006). Radiometric calibration of Landsat data for characterization of early successional forest patterns in western Oregon. *Remote Sensing of Environment*, *103*, 16−26.

Schroeder, T. A., Cohen, W. B., & Yang, Z. (2007). Patterns of forest regrowth following clearcutting in western Oregon as determined from a Landsat time-series. *Forest Ecology and Management*, *243*, 259−273.

Steininger, M. K. (2000). Satellite estimation of tropical secondary forest above-ground biomass: Data from Brazil and Bolivia. *International Journal of Remote Sensing*, *21*, 1139−1157.

Thomas, N. E., Huang, C., Goward, S. N., Powell, S., Rishmawi, K., Schleeweis, K. et al. (in review). Assessment of NAFD forest change products derived from Landsat Time Series Stacks (LTSS). *Remote Sensing of Environment.*

Thompson, J. R., & Spies, T. A. (2009). Vegetation and weather explain variation in crown damage within a large mixed-severity wildfire. *Forest Ecology and Management*, *258*, 1684−1694.

Thornton, P. E., Running, S. W., & White, M. A. (1997). Generating surfaces of daily meteorological variables over large regions of complex terrain. *Journal of Hydrology*, *190*, 214−251.

Tomppo, E. O., Gagliano, C., De Natale, F., Katila, M., & McRoberts, R. E. (2009). Predicting categorical forest variables using an improved k-nearest neighbor estimator and Landsat imagery. *Remote Sensing of Environment*, *113*, 500−517.

Townshend, J. R. G., & Justice, C. O. (1980). Unsupervised classification of MSS Landsat data for mapping spatially complex vegetation. *International Journal of Remote Sensing*, *1*(2), 105−120.

Turner, D. P., Cohen, W. B., Kennedy, R. E., Fassnacht, K. S., & Briggs, J. M. (1999). Relationship between leaf area index and Landsat TM spectral vegetation indices across three temperate zone sites. *Remote Sensing of Environment*, *70*, 52−68.

Wofsy, S. C., & Harris, R. C. (2002). *The North American Carbon Program (NACP): Report of the NACP Committee of the U.S. Interagency Carbon Cycle Science Program.* Washington, D.C.: U.S. Global Change Research Program.

Woodbury, P. B., Smith, J. E., & Heath, L. S. (2007). Carbon sequestration in the U.S. forest sector from 1990 to 2010. *Forest Ecology and Management*, *241*, 14−27.

Woodcock, C. A., Allen, R., Anderson, M., Belward, A., Bindschadler, R., Cohen, W., et al. (2008). Free access to Landsat imagery. *Science*, *320*(5879), 1011.

Zheng, D., Rademacher, J., Chen, J., Crow, T., Bresee, M., Le Moine, J., et al. (2004). Estimating aboveground biomass using Landsat ETM + data across a managed landscape in northern Wisconsin, USA. *Remote Sensing of Environment*, *93*, 402−411.